1-1-2018

Extending Fluspect to simulate xanthophyll driven leaf reflectance dynamics

Nastassia Vilfan
University of Twente

Christiaan Van Der Tol
University of Twente

Peiqi Yang
University of Twente

Rhys Wyber
University of Wollongong, rwyber@uow.edu.au

Zbynek Malenovky
University of Wollongong, zbynek@uow.edu.au

See next page for additional authors

Extending Fluspect to simulate xanthophyll driven leaf reflectance dynamics

Abstract

The xanthophyll cycle regulates the energy flow to photosynthetic reaction centres of plant leaves. Changes in the de-epoxidation state (DEPS) of xanthophyll cycle pigments can be observed as changes in the leaf absorption of light with wavelengths between 500 to 570 nm. These spectral changes can be a good remote sensing indicator of the photosynthetic efficiency, and are traditionally quantified with a two-band physiologically based optical index, the Photochemical Reflectance Index (PRI). In this paper, we present an extension of the plant leaf radiative transfer model Fluspect (Fluspect-CX) that reproduces the spectral changes in a wide band of green reflectance: a radiative transfer analogy to the PRI. The idea of Fluspect-CX is to use in vivo specific absorption coefficients for two extreme states of carotenoids, representing the two extremes of the xanthophyll de-epoxidation, and to describe the intermediate states as a linear mixture of these two states. The 'photochemical reflectance parameter' (Cx) quantifies the relative proportion of the two states. Fluspect-CX simulates leaf chlorophyll fluorescence (ChlF) excitation-emission matrices, as well as reflectance (R) and transmittance (T) spectra as a function of leaf structure, pigment contents and Cx. We describe the calibration of the model and test its performance using various experimental datasets. Furthermore, we retrieved Cx from optical measurements of various datasets. The retrieved Cx correlates well with xanthophyll DEPS (R2=0.57), as well with non-photochemical quenching (NPQ) of fluorescence (R2=0.78). The correlation with NPQ enabled us to incorporate Fluspect-CX in the model SCOPE to scale the processes to the canopy level. Introducing the dynamic green reflectance into a radiative transfer model provides new means to study chlorophyll fluorescence and PRI dynamics on leaf and canopy scales, which is crucial for the remote sensing.

Disciplines

Medicine and Health Sciences | Social and Behavioral Sciences

Publication Details

Vilfan, N., Van Der Tol, C., Yang, P., Wyber, R., Malenovky, Z., Robinson, S. A. & Verhoef, W. (2018). Extending Fluspect to simulate xanthophyll driven leaf reflectance dynamics. Remote Sensing of Environment: an interdisciplinary journal, 211 345-356.

Authors

Nastassia Vilfan, Christiaan Van Der Tol, Peiqi Yang, Rhys Wyber, Zbynek Malenovky, Sharon A. Robinson, and Wouter Verhoef

Extending Fluspect to simulate xanthophyll driven leaf reflectance dynamics

Nastassia Vilfan[a,*], Christiaan van der Tol[a], Peiqi Yang[a], Rhys Wyber[b], Zbyněk Malenovský[b,c,d], Sharon A. Robinson[b], Wouter Verhoef[a]

[a] *University of Twente, Faculty of Geo-Information Science and Earth Observation (ITC), P.O. Box 217, 7500 AE Enschede, The Netherlands*
[b] *Centre for Sustainable Ecosystem Solutions, School of Biological Sciences, University of Wollongong, NSW 2522, Australia*
[c] *Surveying and Spatial Sciences Group, School of Land and Food, University of Tasmania, Private Bag 76, TAS 7001 Hobart, Australia*
[d] *Department of Remote Sensing, Global Change Research Institute CAS, Bělidla 986/4a, CZ-60300 Brno, Czech Republic*

Abstract

The xanthophyll cycle regulates the energy flow to photosynthetic reaction centres of plant leaves. Changes in the de-epoxidation state ($DEPS$) of xanthophyll cycle pigments can be observed as changes in the leaf absorption of light with wavelengths between 500 to 570 nm. These spectral changes can be a good remote sensing indicator of the photosynthetic efficiency, and are traditionally quantified with a two-band physiologically based optical index, the Photochemical Reflectance Index (PRI). In this paper we present an extension of the plant leaf radiative transfer model Fluspect (Fluspect-CX) that reproduces the spectral changes in a wide band of green reflectance: a radiative transfer analogy to the PRI. The idea of Fluspect-CX is to use *in vivo* specific absorption coefficients for two extreme states of carotenoids, representing the two extremes of the xanthophyll de-epoxidation, and to describe the intermediate states as a linear mixture of these two states. The 'photochemical reflectance parameter' (C_{x}) quantifies the relative proportion of the two states. Fluspect-CX simulates leaf chlorophyll fluorescence (ChlF) excitation-emission matrices, as well as reflectance (R) and transmittance (T) spectra as a function of leaf structure,

*Corresponding author. Tel.:+31534893334
Email address: n.rajhvilfan@utwente.nl (Nastassia Vilfan)

pigment contents and C_x. We describe the calibration of the model and test its performance using various experimental datasets. Furthermore, we retrieved C_x from optical measurements of various datasets. The retrieved C_x correlates well with xanthophyll *DEPS* (R^2=0.57), as well with non-photochemical quenching (NPQ) of fluorescence (R^2=0.78). The correlation with NPQ enabled us to incorporate Fluspect-CX in the model SCOPE to scale the processes to the canopy level. Introducing the dynamic green reflectance into a radiative transfer model provides new means to study chlorophyll fluorescence and PRI dynamics on leaf and canopy scales, which is crucial for the remote sensing.

Keywords: `PRI, Fluspect, reflectance, xanthophyll cycle, leaf chlorophyll fluorescence, SCOPE`

2010 MSC: 00-01, 99-00

---

1. Introduction

Under excess irradiance the amount of absorbed photosynthetically active radiation (PAR) exceeds the capacity of photosynthetic reactions, which can cause irreversible damage to the photosystem II reaction centre resulting in photoinhibition. In order to regulate the energy dissipation, photosynthetic eukaryotes have developed many protective mechanisms, in one of which, the excess energy is diverted from the photosystem reaction centres to the pigments of the xanthophyll cycle (Niyogi et al., 1998).

The xanthophyll cycle is an interconversion of three xanthophylls belonging to a carotenoid pigment group: zeaxanthin, antheraxanthin and violaxanthin. Under high PAR levels an increase in the proton gradient across the thylakoid membrane activates the enzymatic conversion of violaxanthin to antheraxanthin and then to zeaxanthin. This interconversion provides a sink for the excess absorbed energy in a process called non-photochemical quenching (NPQ) of chlorophyll fluorescence: the energy is dissipated as heat in the light harvesting complexes associated with photosystem II (Björkman and Demmig-Adams, 1995; Horton et al., 1994; Jahns and Holzwarth, 2012; Niyogi et al., 1998; Ruban,

2016). Under low light conditions or in darkness, the process is readily reversed and zeaxanthin is converted back to violaxanthin.

Numerous studies have shown that NPQ is positively correlated with zeaxanthin formed by the xanthophyll cycle (for reviews, see Demmig-Adams (1990) and Jahns and Holzwarth (2012)).

In practice, the xanthophyll cycle can be observed as dynamic changes in green reflectance between approximately 500 to 570 nm. In order to express these changes with a simple physiologically based optical index, the narrow band photochemical reflectance index (PRI) was defined by Gamon et al. (1992) (for a review, see Garbulsky et al. (2011)). PRI is usually calculated as $(R531 - R570)/(R531 + R570)$, comparing the xanthophyll induced reflectance (R) change at 531 nm to a xanthophyll independent reference band at 570 nm. PRI has been shown to vary significantly over different time scales, in response to different levels of sunlight and to various stresses, from the leaf to the satellite levels. Its empirical relationship to light use efficiency (LUE) has been confirmed over a wide range of species, providing means for global tracking of primary productivity (Garbulsky et al., 2011; Magney et al., 2016; Sims and Gamon, 2002). Moreover, a functional link has been documented between PRI, DEPS of the xanthophyll cycle and NPQ (Evain et al., 2004; Gamon et al., 1992; Peñuelas et al., 1997).

However, the applicability of PRI is limited. In general, correlations are most convincing at the leaf scale, but become far less reliable when we move to the higher levels, due to the influences of canopy structure, viewing and illumination angles on the R signal (Barton and North, 2001; Garbulsky et al., 2011; Zhang et al., 2017).

On the leaf level, the shape of the R signal in the visible range depends primarily on leaf biochemistry. In particular, in the spectral range of 500-570 nm, at least three types of pigments contribute to the shape of the R spectrum, namely chlorophylls, anthocyanins and carotenoids, the later include carotenes and xanthophylls. The absorption spectra of these pigments not only strongly overlap, but also vary with their local chemical environment and scattering

conditions (Lichtenthaler and Buschmann, 2001; Ustin et al., 2009). In order to decouple the individual pigments contributions to the R signal, an index with only 2 bands, such as PRI, is not sufficient.

PRI has been shown to correlate with the ratio of carotenoid to chlorophyll pool sizes. On the diurnal scale it is mostly affected by changes in the xanthophyll cycle, whereas on the longer time scales it primarily depends on the carotenoid and chlorophyll concentration changes (Fréchette et al., 2016; Porcar-Castell et al., 2014; Wong and Gamon, 2015). The use of the index is further complicated by a lack of clear consensus on both the wavelengths used and the normalization methods (Magney et al., 2016; Panigada et al., 2014). A common normalisation method is the use of delta PRI (ΔPRI), calculated by subtracting the dark adapted reference value from the light adapted values. The method is used to measure absolute diurnal as well as seasonal changes in xanthophyll de-epoxidation (Hmimina et al., 2014; Magney et al., 2016).

Besides PRI, few other attempts have been made to model dynamic changes in green R by using the continuous spectral information rather than just two bands (Kováč et al., 2013, 2012), but to our knowledge, a model that can reproduce changes over a broad band of green R in a radiative transfer (RT) manner has never been published.

In this paper, we present an extension to the leaf RT model Fluspect-B (Vilfan et al., 2016), called Fluspect-CX, which is able to reproduce dynamic spectral changes in a broad band of green R, from 500 to 570 nm. Fluspect-CX now provides a dynamic green R together with chlorophyll fluorescence (ChlF) spectrum, using the incoming light and ten parameters as input.

First, we describe a way of calibrating Fluspect-CX specific spectral absorption coefficients (SAC). Next, we present the model routine for retrieving dynamic changes in green R, represented by a parameter C_{x}. We retrieve C_{x} for various datasets and link it empirically to leaf chlorophyll fluorescence dynamics.

Moreover, Fluspect-CX was implemented as a routine within the Soil Canopy Observation of Photosynthesis and Energy (SCOPE) balance model (Van der Tol et al., 2009), and lately also in the three-dimensional Discrete Anisotropic

Radiative Transfer (DART) model (Gastellu-Etchegorry et al., 2017). By including the spectral coefficient for dynamic green R, the leaf model can be up-scaled to the canopy scale, giving the potential to study PRI dynamics in real time at the canopy level.

2. Model description

Fluspect is a radiative transfer model that simulates R and T from 400 nm to 2500 nm and ChlF spectra from 640 nm to 850 nm. It is implemented in Matlab and published under GNU General Public License at `https://github.com/christiaanvandertol`.

Fluspect is based on the model PROSPECT (Jacquemoud and Baret, 1990). Recently, a new version was published, called PROSPECT-D (Féret et al., 2017), which has made a leap further towards modelling leaf optical properties through a complete plant life cycle by introducing anthocyanins as a new model input and re-calibrating the existing SACs of carotenoids and chlorophylls.

Here we present an extension of Fluspect-B (Vilfan et al., 2016), called Fluspect-CX, in which we: 1) incorporate the absorption of anthocyanins and replace the SACs of carotenoids and chlorophylls, as defined in PROSPECT-D and 2) include the SACs for the two extreme states of the violaxanthin de-epoxidation.

The spectral absorption (k) by leaf constituents is simulated in Fluspect by:

$$k(\lambda) = \sum_{i=0}^{n} K_i(\lambda) \cdot C_i \tag{1}$$

where C is the pigment concentration and K the specific spectral absorption coefficient. Fluspect-B uses five SACs (chlorophylls (C_{ab}), carotenoids (C_{car}), leaf water (C_{w}), dry matter (C_{dm}) and senescent material (C_{s})). In Fluspect-CX we incorporate a sixth, representing anthocyanins (C_{ant}), and we add a seventh (C_{x}), which is a radiative transfer analogue to the PRI: it represents the spectral effect of the leaf xanthophyll de-epoxidation, described in the model as

change in the absorption of the total carotenoids. The model input parameters, together with their range and standard values, are defined in Table 1.

Because of the strong overlap of viola- and zeaxanthin absorption spectra with the absorption spectrum of total carotenoids, we could not include them as separate SACs. Instead, we describe the carotenoid absorption spectrum as a linear combination of two coefficients representing the two extreme situations: one for an unstressed leaf, where NPQ and the associated xanthophyll DEPS are 0 (K_{car0}), and one for the state where maximum NPQ activity occurs and DEPS is 1 (K_{car1}):

$$K_{\mathrm{car}} = (1 - C_{\mathrm{x}}) \cdot K_{\mathrm{car0}} + C_{\mathrm{x}} \cdot K_{\mathrm{car1}} \tag{2}$$

where C_{x} is the parameter representing the xanthophyll DEPS.

Table 1: Fluspect-CX input parameters

Parameter	Symbol	Range	Standard value	Unit	Reference	Origin
Chlorophyll a+b content	C_{ab}	0-100	40	µg cm^{-2}	Féret et al. (2017)	PROSPECT-D
Total carotenoid content	C_{car}	0-30	10	µg cm^{-2}	Féret et al. (2017)	PROSPECT-D
Anthocyanin content	C_{ant}	0-10	0	µg cm^{-2}	Féret et al. (2017)	PROSPECT-D
Water content	C_{w}	0-0.4	0.009	cm	Jacquemoud and Baret (1990)	PROSPECT
Dry matter content	C_{dm}	0-0.5	0.012	g cm^{-2}	Jacquemoud and Baret (1990)	PROSPECT
Leaf mesophyll structure parameter	N	1-4	1.4	-	Jacquemoud and Baret (1990)	PROSPECT
Senescence material (brown pigments)	C_{s}	0-0.6	0	fraction in arbitrary units	Jacquemoud and Baret (1990)	PROSPECT
Fluorescence quantum efficiency	η	0-0.2	0.002	-	Miller et al. (2005)	Fluspect
Photochemical reflectance parameter	C_{x}	0-1.5	0	-	/	Fluspect

3. Methodology

The methodology consists of four steps: 1) calibrating the specific spectral absorption coefficients for the total carotenoids representing the two extreme states of violaxanthin de-epoxidation (Section 3.2); 2) developing a protocol for the retrieval of C_{x} from leaf optical measurements (Figure 1, Section 3.3); and 3) performing a sensitivity analysis of a new leaf model (Section 3.4). The experimental data used in each of these steps are presented in Section 3.1.

3.1. Experimental data

Experimental data consists of three datasets. The first dataset (Section 3.1.1) was used for the calibration, and the other two datasets (Sections 3.1.3 and 3.1.4) were used for the validation of the new model. The datasets employ three different measuring techniques, enabling us to evaluate how well C_{x} can be retrieved from different types of measurements. Moreover, Dataset 3 includes high-performance liquid chromatography (HPLC) measurements of carotenes and xanthophylls, allowing us to test the influence of lutein and the xanthophyll $DEPS$ cycle against the retrieved values of C_{x}.

3.1.1. Dataset 1: Transients of reflectance and chlorophyll fluorescence

For the calibration of SACs for the two extreme cases of the violaxanthin de-epoxidation and for quantifying the relationship between C_{x} and fluorescence, we used measurements of leaves in a transient, i.e. dark adapted leaves suddenly exposed to light of a high intensity. The dark adapted starting point assured that the leaf was initially unstressed, and the short duration of the measurements assured that leaf structure and chlorophyll content stayed unchanged. The setup enabled us to study the spectral effects of both $ChlF$ and the xanthophyll de-epoxidation simultaneously. For each leaf we thus obtained the spectrum of R with no NPQ activity (the first spectrum), followed by spectra corresponding to increased violaxanthin de-epoxidation, until the steady state condition (the last spectrum).

The experiment was conducted in the laboratories of Forschungszentrum Jülich in November 2015. R and $ChlF$ measurements were taken on leaves of two bean (*Phaseolus vulgaris* L.) and two sugar beet (*Beta vulgaris* L.) plants. Plants were grown in pots in a greenhouse under controlled conditions; the natural light was complemented with artificial light from growth lamps for 15 hours per day, from 6 am to 9 pm, such that the total light intensity remained relatively stable throughout the day at about 1000 µmol photons m^{-2} s^{-1} (measured in the greenhouse with Li-190SL).

The setup consisted of a spectroradiometer (FieldSpec 4, ASD Inc) connected

to a FluoWat leaf clip. The FluoWat clip is a portable device for standardised bidirectional fluorescence, R and T measurements. The clip has two openings for fibre optics perpendicular to both leaf surfaces (adaxial and abaxial leaf sides) and one light entrance, fitting both a light source at a 45°angle as well as a short-pass filter. For more details on the FluoWat leaf clip design and standard equations used with FluoWat measurements, see **?** and Vilfan et al. (2016). The incident light was filtered with a high performance OD4 short pass filter (TechSpec, Edmund Optics GmbH, Germany), which blocks the irradiance above 650 nm in order to measure ChlF. The samples were illuminated by two different light sources: a cold light lamp (KL 2500 LCD, SCHOTT B.V., The Netherlands) with high illumination of PAR of approximately 1000 µmol photons m^{-2} s^{-1} for bean leaves and 1500 µmol photons m^{-2} s^{-1} for sugar beet leaves, and a custom made LED light source with a lower illumination of PAR around 200 µmol photons m^{-2} s^{-1}.

A dark-adapted leaf was placed in a FluoWat leaf clip, with its adaxial side facing the light source. The R, forward (downward) and backward (upward) $ChlF$ signal (650 to 850 nm) were measured in a transient. The normal operation of the FluoWat clip is to wait for 1-3 minutes after inserting the leaf in the clip before taking measurements, in order to measure the steady state signal. In this experiment, however, we were interested in the transient, i.e. the changes in R and $ChlF$ during the adaptation of the leaf to changed illumination conditions. With each 'transient' we took a sequence of measurements, while the section of the leaf in the FluoWat leaf clip was adapting to provided light exposure; a process that lasted about a minute on average. A measurement was recorded every second. The experiment was repeated with two different light sources on fully developed and attached leaves.

We measured $ChlF$ simultaneously with R spectra by keeping the short-pass filter slotted in front of the light source throughout the experiment. Since our FluoWat was not equipped with a shutter, we briefly switched the light off for a few seconds, while inserting the dark-adapted leaf into the leaf clip. Immediately after inserting the leaf, the lamp was switched on again. Separately, in order to

calculate the true R as well as the filtered transmittance τ, a standard R panel was used to estimate the incident (unfiltered) and filtered radiation.

3.1.2. Estimation of fluorescence quenching

For Dataset 1, we estimated NPQ from the $ChlF$ measurements. In practice, it is not possible to objectively distinguish the effects of NPQ and photosynthetic quenching (PQ) on ChlF without a separate measurement technique, such as pulse amplitude modulation (PAM) fluorometry. However, theoretically it can be separated when considering the rate coefficients (K_p and K_n for PQ and NPQ, and K_d and K_f for heat dissipation and fluorescence, respectively, as in Van der Tol et al. (2014)):

$$F(t) \propto Q \cdot \frac{K_f}{K_f + K_d + K_p + K_n}, \tag{3}$$

where $F(t)$ represents fluorescence in absolute units in time and Q is the light intensity.

The rate coefficients K_f and K_d can be considered as constants (we set K_f+$K_d = 1$), but K_p and K_n are variable. At the first measurement ($F_t = 0$) we assume $K_n = 0$, and fluorescence can be expressed as:

$$F(t = 0) \propto Q \cdot \frac{K_f}{K_f + K_d + K_{p0}}. \tag{4}$$

Next, we combine eqs. 3 and 4 into their ratio and express the change in fluorescence as:

$$\frac{F(0)}{F(t)} - 1 = \frac{K_n + (K_p - K_{p0})}{1 + K_{p0}}. \tag{5}$$

In order to estimate the quenching effects, we assumed that at the first measurement K_{p0} was also zero. The combined effect of K_p+K_n can then be expressed as:

$$K_p + K_n = (\frac{F(0)}{F(t)} - 1) \tag{6}$$

where K_n+K_p can be calculated from the first measurement of fluorescence (F(0)) and any other measurement at time t (F(t)) during the transient.

3.1.3. Dataset 2: Diurnal cycles of fluorescence and reflectance in avocado and orange jasmine leaves

For validation of retrievals of C_x, we used measurements performed on fully expanded leaves of two C3 plants, avocado (*Persea americana* Mill. cv. Haas) and orange jasmine (*Murraya paniculatta* Jack) at the University of Wollongong, Australia in April, September and November 2015. Six leaves of either orange jasmine or avocado were monitored over 18 diurnal cycles throughout the year (10 diurnal cycles of avocado and 8 diurnal cycles of orange jasmine) (for detailed description of growth conditions and measurements see Wyber et al. (2017)). Additionally, it should be noted that unlike other plants used in this study, avocado leaves have both a xanthophyll and a lutein epoxide cycle. In deep shade avocado leaves, lutein slowly converted to lutein epoxide, which is readily converted back to lutein under strong light (Matsubara et al., 2005). However, the avocado leaves used in this experiment were either full sun exposed leaves, or outer canopy leaves receiving diurnal PAR intensities greater than that would allow for significant accumulation of lutein epoxide.

Measurements of diurnal changes in leaf reflectance and both active and passive ChlF were taken on leaves fixed in a vertical position in the perpendicular distance of 1 m from the sensor head. Active chlorophyll fluorescence was measured using a commercially available Light Induced Fluorescence Transient instrument (LIFT) (Soliense Inc, Shoreham, NY, USA; `http://www.soliense.com/LIFT_Terrestrial.php`). A cross-comparison of LIFT and PAM (mini-PAM; Walz, Effeltrich, Germany) measurements during light response curves proved their reciprocal comparability ($R^2 = 0.90$ for ϕ_{II}). Leaf radiance was measured with a QE Pro (Ocean Optics, Dunedin, FL, USA) spectroradiometer with a spectral range of 440 to 870 nm and spectral resolution of 0.7 nm. Both instruments observed leaves with the same field of view and each measurement consisted of a QE Pro single leaf reflected radiance measurement, followed by a LIFT measurement.

In our study, we used a total of 7 samples of diurnal cycles: 4 avocado and

3 orange jasmine leaves. Leaf reflectance spectra with high errors, particularly due to clouds and the shading of the instruments were filtered out from the dataset. Because the leaves were fixed in a vertical position, the R signal was highly influenced by the solar illumination angle, resulting in strong directional effects. In order to minimize these effects, we normalized the spectra to 565 nm. We chose this wavelength on the basis of where the xanthophyll cycle ceases to have any spectral effect in the Fluspect model.

3.1.4. Dataset 3: Reflectance measurements in an integrating sphere and pigment dynamics of avocado leaves

Fully expanded leaves of the avocado plants, which were used also for Dataset 2 (Section 3.1.3), were prepared the evening prior to the laboratory experiment by cutting and transferring their petiole into a centrifuge tube containing 10 ml of water. This transfer was conducted under room temperature to avoid air entering the leaf xylem. Parafilm was used to provide a water tight seal between a hole in the centrifuge tube lid and the leaf petiole. Following the collection, leaves were allowed to dark adapt overnight prior to experiments performed the following day.

Pigment dynamic experiments were performed between the 4th to the 26th of June 2015, with leaves randomly sampled from the available plants. Detached avocado leaves were mounted horizontally with the abaxial leaf surface in contact with a corrugated cardboard surface as to not block leaf stomata. As a control, one half of each leaf was covered with non-transmissible black fabric and the other half was treated with 800 or 600 μmol photons m^{-2} s^{-1} of white light from a warm white incandescent reflector bulb (Philips Electronics Australia). To limit the impact of heat produced by the incandescent bulb, a large Petri dish filled with 40 ml of distilled water was suspended just above leaf surfaces. Leaf surface temperatures were recorded with a TiS10 Infrared Camera (Fluke Australia Pty Ltd), using the emissivity of 0.98. Leaf temperatures were found to increase by approximately 2°C following light treatment, with no significant difference between the control and light treated leaf regions. Irradiance at the

leaf surface was measured using a MQS-B Cosine Corrected Mini Quantum Sensor and ULM-500 light metre (Heinz Walz GmbH, Germany), with the sensor head placed at the level of the leaf surface. Leaf optical properties, light response curves and leaf hole punches were collected from both the control and treated leaf section before the light treatment, immediately after the treatment and two hours post the treatment. Leaf optical measurements were performed using a Li-COR integrating sphere (Li-COR 1800-12S, Li-COR, Inc., Lincoln, Nebraska, USA) coupled via a 400 µm optical fibre with a QE Pro spectroradiometer (Ocean Optics, Florida, USA). Measurements were acquired between 440 to 870 nm at a 0.7 nm spectral resolution using a 280 ms integration time and six averaged spectral scans. Leaf R and T for both abaxial and adaxial leaf surfaces were measured as described in the Li-COR 1800 portable spectrometer manual (Li-COR 1800-12S, Li-COR, Inc., Lincoln, Nebraska, USA), using a comparable separate avocado leaf to account for the sample substitutional error. Three independent spots on leaf blades (marked using a permanent marker) were measured on both control and treated sections for each leaf.

Light response curves were measured on both control and treated leaf sections using a miniPAM and a 2035-B leaf clip (Heinz Walz GmbH, Germany) on a separate spot to those used to measure leaf optical properties. They were performed using nine irradiance steps from 0 to 600 µmol photons m^{-2} s^{-1}, with two minutes at each illumination level and a five step dark recovery over five minutes.

HPLC pigment analysis was performed on leaf hole punches collected from both control and treated leaf section at each point in time. Pigments were analysed on equipment described in Wyber et al. (2017), using the methodology outlined in the former and based upon the methods of Pogson et al. (1996).

The $DEPS$ was calculated using the formula:

$$DEPS = \frac{Antheraxanthin + Zeaxanthin}{Antheraxanthin + Zeaxanthin + Violaxanthin} \tag{7}$$

In our study, we used all samples, which had combined measurements of leaf R or T, NPQ and $DEPS$, i.e. 9 leaves in total. Data did not undergo any

additional processing.

3.2. Calibration of the specific absorption coefficients for xanthophyll de-epoxidation

The calibration for the two SACs representing the two extreme states of total carotenoids due to the xanthophyll de-epoxidation, K_{car0} and K_{car1}, was carried out with the numerical optimization routines using the measured leaf R, similar to the procedure described in Féret et al. (2017). We selected the transients of one sugar beet and two bean leaves from Dataset 1 for the calibration, and reserved the remaining 8 transients (6 bean and 2 sugar beet samples) for validation purposes.

The calibration procedure consisted of the following steps: 1) We retrieved the values of PROSPECT parameters (see Table 1) from the last R spectrum of the transient over the spectral range of 400 to 1800 nm by using the K_{car}, K_{ab} and K_{ant} as defined in PROSPECT-D. 2) We calibrated K_{car} to the first (unstressed) R spectrum of all the three leaves simultaneously, thus obtaining K_{car0}. 3) We re-calibrated K_{car} to the last R spectrum of all the three leaves simultaneously by setting $C_{\mathrm{x}} = 1$ for the last measurements, thus obtaining K_{car1}.

In all three steps, the Matlab built-in function 'lsqnonlin' was applied, to minimize a cost function:

$$C = (M - S)^2 \tag{8}$$

where M are the measured R spectra and S the corresponding simulation spectrally convolved to the resolution of the spectroradiometer. In the calibration steps 2 and 3, M and S were matrices of three leaves (i.e. three R spectra in total). In these steps, all the parameters were kept constant at their retrieved values and both SACs were constrained to be positive.

3.3. Retrieval of C_x

In order to accurately estimate C_{x}, we evaluated different retrieval methods.

We assumed all PROSPECT parameters to be constant in time during the measurements. We retrieved the PROSPECT parameters for the first spectrum

only, and kept them constant for all other spectra of the same measurement sequence. C_{x} was then retrieved separately for the starting spectrum, as well as all other spectra of the same leaf. The same cost function was applied as in the calibration, as described above (Section 3.2).

While retrieving all PROSPECT parameters over the whole measured spectral range, it became evident that the model could not sufficiently accurately reproduce the measurements in the visible and near infra-red range simultaneously. Consequently, the final configuration of the retrieval was established in 3 steps (Figure 1): 1) For the first (unstressed or reference) spectrum of the measurement, we retrieved all PROSPECT parameters over the whole measured spectral range. 2) For the reference spectrum, we retrieved the PROSPECT parameters with the main absorption in the visible spectrum (VIS) over the VIS range, while keeping the parameters with the main absorption in the near-infra red fixed at the values acquired in the first step. This step was introduced to improve the fit in the range relevant for the retrieval of C_{x}. 3) C_{x} was retrieved separately over the range of 520 - 565 nm, while keeping all other parameters constant at their previously retrieved values for the reference leaf.

For all three datasets, we retrieved C_{x} by fitting only reflectance, with the exception of Dataset 3 (Section 3.1.4, where we retrieved C_{x} by fitting either reflectance, transmittance, or both at the same time. We evaluated the retrieval accuracy for each dataset with the relative root mean-squared error (RRMSE). The retrieved C_{x} values were further compared to NPQ, as well as lutein and xanthophyll DEPS measurements of the same leaves, where available, by calculating the root mean-squared error (RMSE) and Pearson's correlation coefficient (R^2) as measures for the goodness-of-fit.

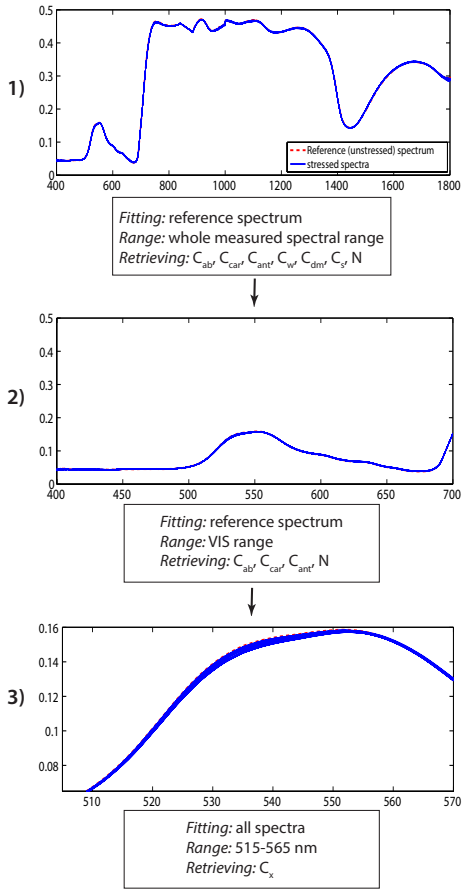

Figure 1: Diagram of the C_{x} retrieval process: Top: model fit for the VNIR region. Middle: improved model fit for only the VIS region. Bottom: model fit after retrieving C_{x}.

3.4. Model sensitivity and error propagation

In order to investigate the most influential parameters for R, and also the ill-posedness of their retrieval, we calculated the Jacobian (J) matrix of the model for one representative sample, and locally linearised the model:

$$\Delta R = J\Delta p \tag{9}$$

where J is a matrix with the partial derivatives of the R at each wavelength (rows) for each of the 8 parameters (columns), here restricted to the VIS. Eq. 9

describes the propagation of a small change in the parameter vector (Δp) into the reflectance (ΔR).

To obtain comparable values of the sensitivities and to normalise J_N, we multiplied J by the span of each parameter (see Table 1). Subsequently, we carried out Singular Value Decomposition (SVD) of J_N:

$$J_N = U\Sigma V^\top \tag{10}$$

where Σ is a diagonal matrix of non-negative real singular values, and the columns of U and V are the left-singular vectors and right-singular vectors of J_N, respectively. U is a matrix of 8 spectra, and V is a 8×8 matrix providing the contributions of each of the 8 parameters to each spectrum in U. The occurrence of relatively low singular values indicates ill-posedness.

To compute the error propagation (i.e., the standard deviation (SD)) in the retrieval of model parameters, we inverted Eq. 9:

$$J^\top \Delta R = J^\top J \Delta p, \tag{11}$$

and wrote Δp as a function of ΔR:

$$\Delta p = (J^\top J)^{-1} J^\top \Delta R. \tag{12}$$

A covariance matrix of p as a result of noise in R is:

$$\begin{aligned} &E(\Delta p \Delta p^\top) = E[(J^\top J)^{-1} J^\top \Delta R \Delta R^\top J (J^\top J)^{-1}] \\ &= (J^\top J)^{-1} J^\top E(\Delta R \Delta R^\top) J (J^\top J)^{-1}, \end{aligned} \tag{13}$$

where $E(\Delta R \Delta R^\top)$ is the covariance matrix of the measurements. If this covariance matrix is diagonal and uniform (all diagonal elements equal), characterized by a variance σ_r^2, then the covariance matrix of the retrieved parameters due to measurement noise is given by:

$$\begin{aligned} &E(\Delta p \Delta p^\top) = (J^\top J)^{-1} J^\top \sigma_r^2 J (J^\top J)^{-1} \\ &= (J^\top J)^{-1} J^\top J (J^\top J)^{-1} \sigma_r^2 \\ &= (J^\top J)^{-1} \sigma_r^2. \end{aligned} \tag{14}$$

The standard deviations of the retrieved parameters (σ_p) are then found as the square roots of the diagonal elements of this matrix. For σ_r we used the value of the signal mean divided by the signal to noise ratio (SNR) of 500, and calculated Δp.

4. Results

4.1. Specific absorption coefficient spectra

In the left panel of Figure 2, we compare the SACs for carotenoids, chlorophylls and anthocyanins of PROSPECT-D with those of PROSPECT-5 (Féret et al., 2008), which were originally used in Fluspect-B. K_{car} differs mostly in the wavelengths below 500 nm, whereas the two versions for K_{ab} demonstrate substantial differences throughout the spectrum. Results of Féret et al. (2017) show a great improvement in retrieval accuracy when using PROSPECT-D coefficients compared to older versions, and thus appear more useful.

In the middle panel of Figure 2, we plot the SACs for the two extreme states of carotenoids, K_{car0} and K_{car1}, which now replace K_{car} originating from PROSPECT-D. The K_{car0} spectrum is shifted by approximately 2 nm into the shorter wavelengths compared to K_{car}. The difference between the two spectra (the right panel of Figure 2) has a maximum at 528 nm, and gradually diminishes towards 500 nm and 565 nm.

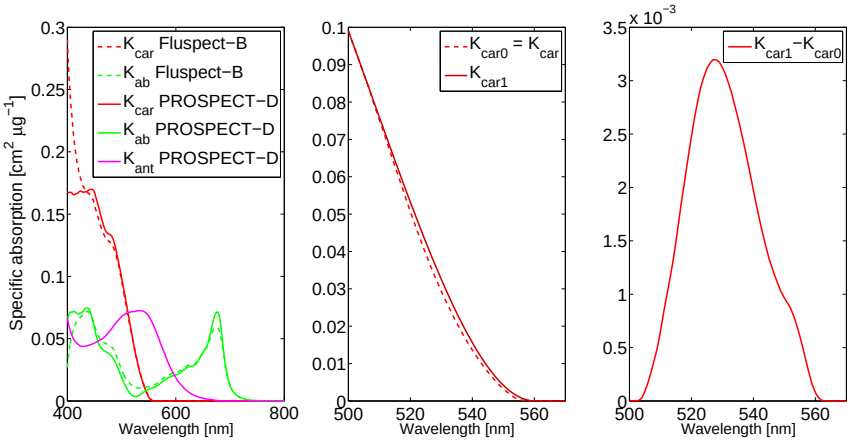

Figure 2: Specific absorption coefficients for: carotenoids (K_{car}), chlorophylls (K_{ab}) and anthocyanins (K_{ant}) as adopted from PROSPECT-D (solid line) compared to the version used in Fluspect-B (broken line) (left panel); the two extreme states of carotenoids, K_{car0} (broken line) and K_{car1} (solid line) as defined in Fluspect-CX, displayed in the range of 500 to 570 nm (middle panel); difference between the two extreme states of carotenoids (right panel).

4.2. Dynamics of measured reflectance and ChlF spectra

Dataset 1 provided with unique data on simultaneous changes of $ChlF$ and green R. We observed the induction of $ChlF$ at the first second after exposing the leaf to illumination, and then a gradual decrease over about a minute, due to photochemical and non-photochemical quenching. NPQ dynamics can be observed by a gradual decrease in the green R that closely accompanies the changes in $ChlF$. The dynamics of the two responses and their relation are presented for a representative sample in Figure 3.

4.3. Parameter retrieval

A representative measured and fitted spectrum for each of the two extreme states is presented in Figure 4. As expected from the optical coefficients, we observe the maximum spectral differences between the two extreme spectra in the transient between 525 and 550 nm, and diminishing differences before 510 and beyond 560 nm.

In the left top panel of Figure 4 we show the spectra of Fluspect after fitting PROSPECT parameters with PROSPECT-5 coefficients (steps 1 and 2 of Section 3.3), illustrating that the spectral fit is insufficiently accurate to retrieve C_{x}. In the right panels we used PROSPECT-D coefficients, K_{car0} and K_{car1} following all three steps: retrieving PROSPECT-D parameters as well as C_{x} for the first spectrum, but only C_{x} for the last. With these coefficients, the spectral fit can be considered as sufficient.

The middle and the bottom panels of Figure 4 show the relative root mean square error (RRMSE) of retrieval accuracy per dataset. It is evident, that when retrieving from VIS and NIR spectra simultaneously (bottom panels), the region between 500 and 600 nm cannot be reproduced accurately (RRMSE of up to $\pm 20\%$), and the step 2 of Section 3.3 is indeed required. When retrieving C_{x} over the spectral range of 500 to 600 nm, the accuracy is generally very good (RRMSE of $\pm 1\%$), except below 520 nm, where the model cannot reproduce the measurements well.

We conclude that Fluspect-CX reproduces the R between 520 and 570 nm more accurately, in contrast to Fluspect-B, where a significant discrepancy between the measured and fitted spectra is evident throughout the spectral region affected by the xanthophyll cycle (maximal RRMSE of $\pm 8\%$).

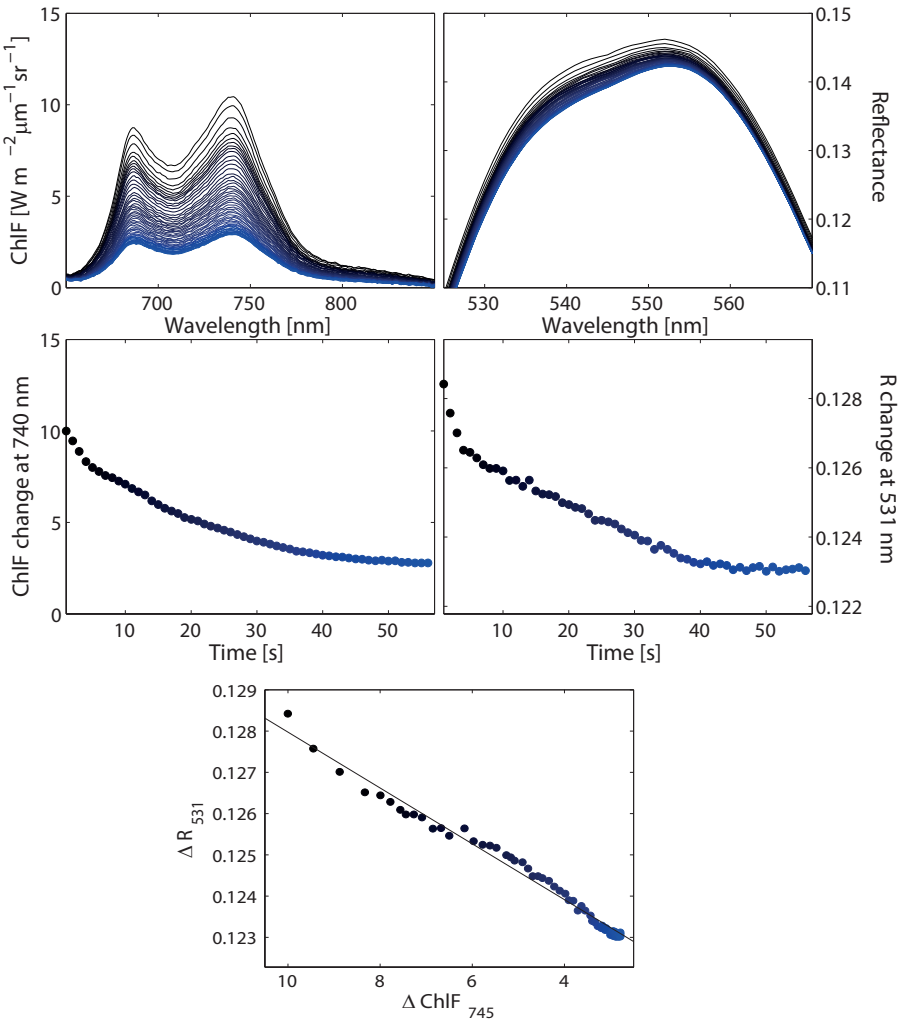

Figure 3: Dynamics of measured ChlF and green R spectra, plotted against wavelength (upper panels) or as change in time (middle panels) for one representative sample. Bottom panel displays the change in green R at 531 nm as a function of ChlF at 745 nm ($R^2 = 0.98$).

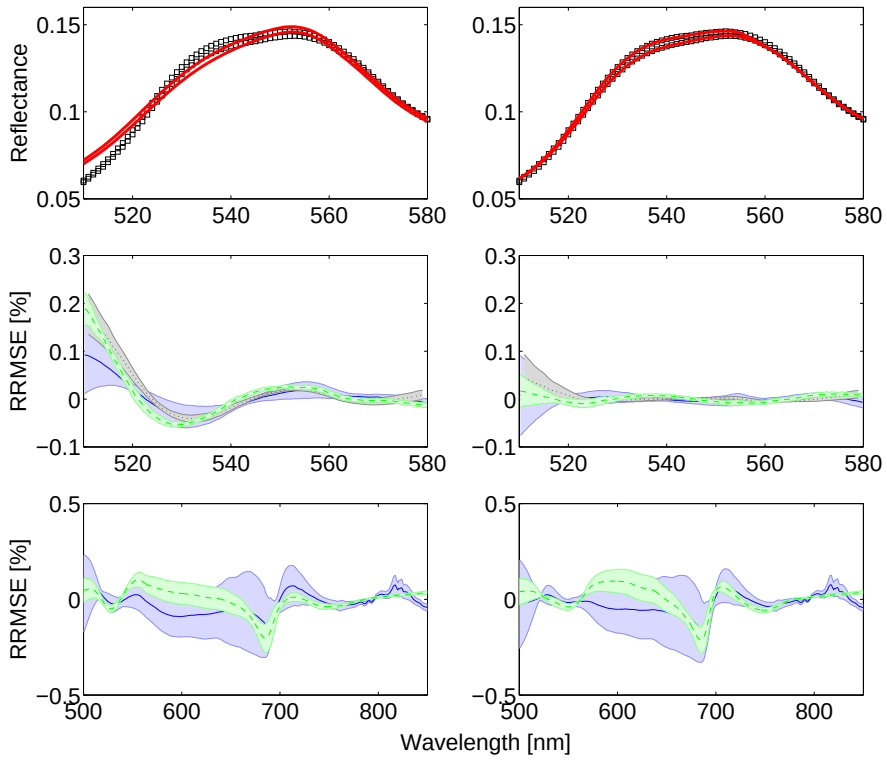

Figure 4: Comparison of the measurements and the retrieval accuracy of either Fluspect-B (left panels) or Fluspect-CX (right panels). Top panels show measured (squares) and fitted spectra (solid line) between 510 and 580 nm. In the middle and bottom panels we plot the relative root mean square error (RRMSE) of retrieval accuracy after fitting between 500 and 580 nm (middle panels) and after fitting over VIS and NIR (bottom panel). Shaded area represents the standard deviation of the mean. The three colours represent three datasets: dotted line (black) for Dataset 1, whole line (blue) for Dataset 2 and broken line (green) for Dataset 3.

4.4. Dynamics of ΔPRI, C_x and NPQ

For a further validation of the C_x retrievals, we investigated relationships among C_x, ΔPRI and NPQ using all three datasets. By plotting C_x and ΔPRI versus NPQ, we obtained the empirical relationships (Figure 5). The relationship between C_x and NPQ can be described by a linear equation. Goodness of fit represented by Pearson's correlation coefficient (R^2; Table 2) is generally better for $NPQ(C_\mathrm{x})$ (R^2=0.78) compared to $NPQ(\Delta PRI)$ (R^2=0.30) for all datasets combined. Moreover, $NPQ(\Delta PRI)$ performs slightly better in the case of the data acquired with the integrating sphere, whereas for diurnal data $NPQ(C_\mathrm{x})$ relationship significantly outperforms $NPQ(\Delta PRI)$.

Retrieval of C_x for R, T and R+T simultaneously for the integrating sphere data shows, that the model can reproduce the effect similarly well (R^2≈0 .58) for all three scenarios.

Light source intensity does have a significant influence on the span of C_x: the higher the illumination is the higher the values of NPQ (or K_p+K_n) are, as evident from the diurnal data and the transient data measured with the much brighter halogen lamp.

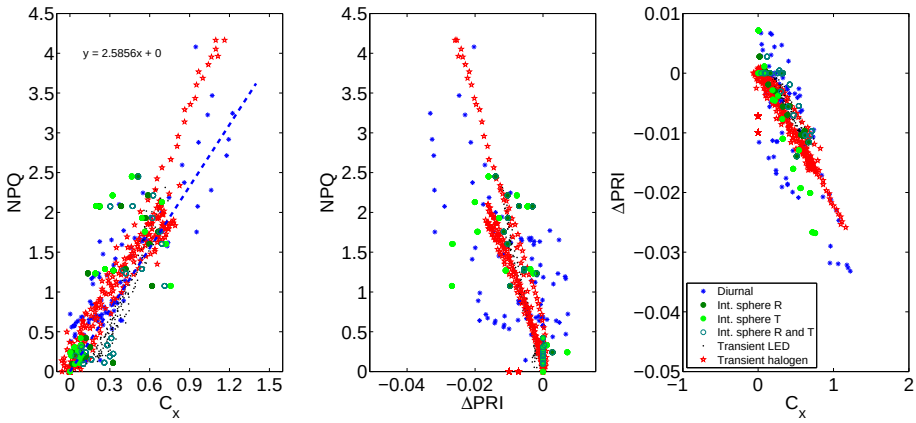

Figure 5: Relation of NPQ (K_p+K_n for Dataset 1) to C_x (left) and ΔPRI (middle), as well as ΔPRI to C_x (right). Different symbols and colours mark different datasets. The blue dashed line in the left panel represents the least squares linear relationship between C_x and NPQ, determined for Datasets 2 and 3 combined.

Table 2: Statistical data supporting Fig.5. Pearson's correlation coefficient (R^2) and RMSE are represented per dataset.

	NPQ($C_\mathbf{x}$)		**NPQ(ΔPRI)**		**ΔPRI($C_\mathbf{x}$)**	
	R^2	RMSE	R^2	RMSE	R^2	RMSE
Diurnal	0.54	0.451	0.10	0.634	0.60	0.008
Int. sphere R	0.60	0.538	0.76	0.420	0.88	0.002
Int. sphere T	0.53	0.598	0.45	0.651	0.95	0.002
Int. sphere R and T	0.58	0.556	0.76	0.420	0.77	0.002
Transient LED	0.91	0.188	0.96	0.129	0.90	0.001
Transient halogen	0.94	0.240	0.57	0.645	0.61	0.004
All combined	0.78	0.388	0.30	0.692	0.49	0.005

In Figure 6 we explore the effects of pigment dynamics on C_x and NPQ. C_x dynamics can be statistically related to the $DEPS$ (R^2=0.57), whereas, interestingly, NPQ cannot (R^2=0.21). As demonstrated, lutein epoxide has a non-systematic effect on C_x.

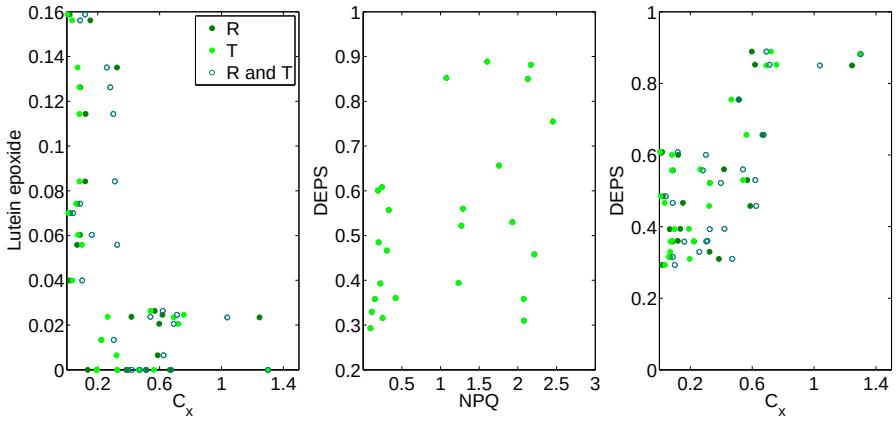

Figure 6: Dependence of C_x on lutein epoxide (left; $R^2 = 0.31$), NPQ on de-epoxidation status (DEPS; $R^2 = 0.21$) (middle) and C_x on DEPS (right; $R^2 = 0.57$). Data for retrievals of C_x from R, T and R+T are presented separately, where applicable.

4.5. Model sensitivity

Figure 7 and Table 3 show a representative example of the SVD, computed for a normalized Jacobian of the reflectance model, restricted to the visible spectrum. As expected, the highest SVs are dominated by parameters for photosynthetic pigments, with the highest contributions of C_{ab}, C_{car} and C_{ant}, to each of the first three SVs, respectively.

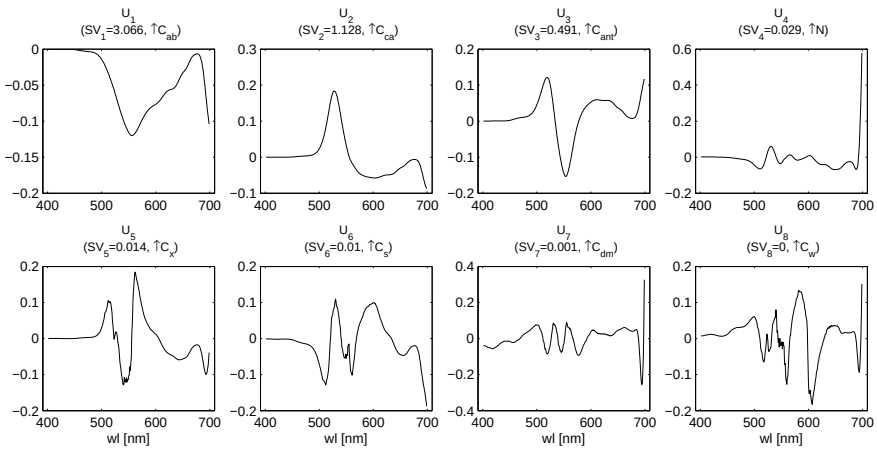

Figure 7: Left singular vectors (U) for the Jacobian of the reflectance model for one representative sample, narrowed down to the visible spectrum. The singular value (SV), t.i. the weight of the vector, and the most contributing parameter (↑parameter) are provided in the caption of each sub-plot. Refer to Table 3 for the right singular vectors (V), the SV and rank of each of the 8 parameters.

The fourth to eight SVs represent less than 1% of the first value, and the influence of other parameters, including C_{x}, becomes more important.

C_{x} fully dominates the fifth SV, which represents only 0.5% of the highest SV. Nonetheless, this indicates that the contribution of C_{x}, however small, is unique. Moreover, the left singular vector for C_{x} (U_5 in Figure 7) suggests that for the retrieval of C_{x} one might need to consider spectral differences at 3 highly specific wavelengths: 512, 539 and 562 nm.

The sixth SV is dominated by C_{s}, with a noticeable contribution of C_{x}. The seventh is dominated by C_{dm}. The eighth is again an order of magnitude

smaller than the seventh, as is dominated by water absorption, which does not occur in the VIS part of the electromagnetic spectrum.

Furthermore, the first four SVs are dominated by parameters with contributions of the opposite sign, which indicates that the spectral effects of these parameters can, to some degree, cancel each other out, resulting in potential over- or underestimations of these parameters.

The retrieved parameter values (RV) and the error propagation in the retrieved parameters (σ_p) in the VIS are presented in Table 4. σ_p ranges from about $\pm 10\%$ of the retrieved values for C_{ab}, C_{car} and N, to a very high value for C_{w}. This is expected, as C_{w} cannot be principally estimated from the VIS wavelengths. On the other hand, the error propagation for C_{x} is the lowest, about $\pm 3\%$, due to the low sensitivity of the model to C_{x}.

Table 3: Singular values (SV) and right singular vectors (V) of the Jacobian matrix for the reflectance model after fitting to the measured reflectance of a sugar beet leaf, narrowed down to the visible spectrum. The highest contribution per SV is shown in bold font. The squared sum over rows equals 1, and the squared sum over columns equals 1.

SV	3.066	1.128	0.491	0.029	0.014	0.010	0.001	0.000
Rank	1	2	3	4	5	6	7	8
$C_{\mathbf{ab}}$	**0.77**	0.46	-0.12	0.36	-0.00	-0.09	0.22	0.00
$C_{\mathbf{dm}}$	0.06	-0.03	0.06	-0.55	-0.03	0.00	**0.83**	0.00
$C_{\mathbf{w}}$	0.00	0.00	-0.00	-0.00	0.00	0.00	-0.00	**1.00**
$C_{\mathbf{s}}$	0.07	-0.08	0.12	-0.17	-0.46	**-0.85**	-0.14	0.00
$C_{\mathbf{ca}}$	0.13	**-0.72**	-0.58	0.30	-0.03	-0.08	0.20	0.00
N	-0.54	0.19	0.15	**0.63**	-0.04	-0.22	0.45	0.00
$C_{\mathbf{x}}$	0.01	-0.03	0.01	-0.08	**0.88**	-0.46	-0.02	-0.00
$C_{\mathbf{ant}}$	0.30	-0.48	**0.78**	0.22	0.05	0.10	0.05	0.00

Table 4: Retrieved values (RV) after fitting to the measured reflectance and the retrieval error propagation (σ_p) in the visible spectrum, assuming a signal to noise ratio of 500. The lower (LB) and upper (UB) boundaries are calculated as RV$\pm\sigma_p$; LB are constrained to 0.

	RV	σ_p	**LB**	**UB**
$C_{\mathbf{ab}}$	34.80	3.74	31.06	38.53
$C_{\mathbf{dm}}$	0.014	0.005	0.009	0.019
$C_{\mathbf{w}}$	0.012	0.700	0.000	0.712
$C_{\mathbf{s}}$	0.000	0.017	0.000	0.017
$C_{\mathbf{ca}}$	9.77	1.03	8.74	10.80
N	1.41	0.16	1.25	1.56
$C_{\mathbf{x}}$	0.62	0.02	0.60	0.64
$C_{\mathbf{ant}}$	0.56	0.09	0.46	0.65

5. Discussion

5.1. Photochemical reflectance in Fluspect

By means of adding calibrated SACs for two extreme states of the carotenoid absorption spectrum, namely K_{car0} and K_{car1}, we have included the PRI effect in Fluspect.

According to our results, several features indicate that K_{car0} and K_{car1} describe the xanthophyll DEPS of plant leaves. Both of the calibrated SACs, and also the measured spectra for the two extreme states show a similar shift with a maximum between approximately 525 and 550 nm (Figs. 2 and 4). Moreover, the difference curve of the two SACs has a peak at 528 nm. These values are in accordance with previous reports (Gamon et al., 1992, 1997; Hmimina et al., 2014; Kováč et al., 2013). Furthermore, the experimental setup used in the calibration assured that constitutive leaf properties, i.e. irreversible slow changes in leaf pigment content and anatomy, had stayed the same during the experiment. The change in green reflectance during a transient could then be ascribed primarily to the change in the violaxanthin de-epoxidation status.

Retrieved values of C_{x} are strongly related to both ΔPRI and $DEPS$ (Figs. 5 and 6, respectively). PRI has been been shown to correlate with $DEPS$ similarly as C_{x}, with R^2 between 0.5 to 0.7, for needle- (Fréchette et al., 2016;

Harris et al., 2014) and broad-leaved species (Gamon et al., 1990), at the leaf scale over short (diurnal) time scales.

Similarly, both ΔPRI and C_{x} display a comparable general relationship with NPQ (Fig. 5 and Table 2), albeit reversed: increasing C_{x} predicts an increase in NPQ.

It is not surprising that the dependence of C_{x} on $DEPS$ is much higher than the dependence of NPQ on $DEPS$: NPQ measured by PAM methods is a combination of ΔpH of the thylakoid, xanthophyll de-epoxidation cycle, changes in constitutive losses and many other quenching effects (Ruban, 2016). NPQ is triggered by ΔpH either directly, or indirectly, by the activity of the xanthophyll cycle(s). Nonetheless, the high correlation between C_{x} and NPQ suggests, that C_{x} might represent more factors involved in the dynamics of green R, than the de-epoxidation of violaxanthin alone.

On a diurnal scale, C_{x} represents the xanthophyll DEPS within the leaf, with a value of C_{x} equal to zero corresponding to the case where no zeaxanthin dependent NPQ is active and the associated xanthophylls still consist entirely of violaxanthin. On the other hand, a value of approximately 1 corresponds to the situation where maximum NPQ activity occurs and violaxanthin undergoes full de-epoxidation. We acknowledge, that K_{car1} is likely underestimated: In *in vivo* leaves of higher plants, maximal DEPS is variable but never 100%, as well as species and growth light conditions dependant (Adams and Demmig-Adams, 1992; Demmig-Adams and Adams, 2006). As such, the SAC for maximum DEPS is difficult to characterize by using *in vivo* measurements. In our results, the upper limit was not set as a hard boundary and the estimated values of C_{x} extended slightly beyond 1, up to approximately 1.2, suggesting that the samples we used for K_{car1} calibration were not fully de-epoxidized.

When measuring leaf spectra throughout the day in a natural, uncontrolled environment, changes in green R are subjected to more than just the xanthophyll cycle change, for example changes in light direction, chloroplast movements, lutein epoxide cycle, temperature stress, water stress etc. It is likely that some of the mentioned features are present in the calibrated spectrum, even though

the model does not take them into account explicitly.

Some of these effects vary greatly with changing leaf anatomy, among species or with plant functional types. Such an example are chloroplast movements (Brugnoli and Björkman, 1992; Königer and Bollinger, 2012; Suetsugu et al., 2017), and lutein epoxide cycle (García-Plazaola et al., 2007). Contrary to these photoprotective plant mechanisms, the xanthophyll cycle is known to be present in all plant-like eukaryotes, from algae to higher plants (Niyogi et al., 1998).

In addition to the xanthophyll cycle, the lutein epoxide cycle can also contribute to the dissipation of excess absorbed light energy (Demmig-Adams, 1990; Gilmore and Yamamoto, 1993; Niyogi et al., 1997). Lutein epoxidation is mostly restricted to woody species, such as avocado, used in this study, and accumulation of lutein epoxide to high concentrations is found most commonly in old leaves in deeply shaded canopies (García-Plazaola et al., 2007). Results of our study suggest that lutein epoxidation had a minimal effect on the dynamics of green reflectance, the most likely reason being the conditions in which the avocado plants were grown. Consequently, the lutein-epoxidation might not have been active and therefore the influence of the lutein epoxide cycle on the experiments was limited. Leaves with a lutein epoxide cycle have a photo-active and constitutive level of lutein (García-Plazaola et al., 2007). The lutein epoxide measured was thus likely a part of the constitutive pool. Moreover, recent progress of research on the roles of zeaxanthin and lutein in photoprotection of photosystem II also indicates that Z is the major player in NPQ (Jahns and Holzwarth, 2012).

Over seasonal time frames, green R is further affected by slowly changing (constitutive) components, such as variations in pigment (chlorophyll, carotenoid and anthocyanin) pool sizes; and PRI is primarily controlled by carotenoid and chlorophyll content rather than xanthophyll cycle dynamics (Fréchette et al., 2016; Gitelson et al., 2017). Also, the ideal reference waveband for PRI varies between experiments and treatments (Gamon et al., 1992; Panigada et al., 2014). Due to the strong overlap of the absorption features of different pigments in the

VIS, indices using only one or two spectral bands may be insufficient to decouple rapidly changing (facultative) and slowly changing (constitutive) components. In the case of PRI, Hmimina et al. (2014) and Magney et al. (2016) showed that the use of a reference ΔPRI, defined as the PRI of perfectly dark-adapted leaves, is needed in order to be able to separate the physiologically related PRI variability over both diurnal and temporal scales.

RT models have an advantage, that they allow an analysis of the remote sensing signal based on robust physical, chemical, and biological processes. The relations between biochemical parameters and spectral reflectance are expected to be independent of site conditions and do not require field data for input after calibration. In fact, they represent an ideal tool to develop and test optical indices (Haboudane et al., 2002; Malenovský et al., 2006). Our results support this: retrieved values of C_{x} appeared to be better comparable among leaves of different datasets than ΔPRI (Table 2).

5.2. Retrieval of Cx: requirements, sensitivity and limitations

The inclusion of re-calibrated SACs for carotenoids, chlorophylls and anthocyanins of PROSPECT-D greatly improved the accuracy of retrieval, reported also by the other studies (Féret et al., 2017; Li et al., 2018).

Accurate determination of *in vivo* SACs is critical. Although *in vitro* SACs from isolated pigments in solutions are available in literature, their inclusion in leaf radiative transfer models is complicated by three factors: (1) the absorption spectrum of a pigment depends on the choice of sample, solvent system, and spectrophotometer used (Lichtenthaler and Buschmann, 2001); (2) similarly, the *in vitro* SACs will clearly differ from the *in vivo* SACs of the pigments in the natural leaves; (3) the absorption features of different pigments strongly overlap in the VIS. This is especially true for the major carotenoids of green leaves, such as β-carotene, lutein, neoxanthin and violaxanthin (Lichtenthaler and Buschmann, 2001).

The overlap makes it difficult to correctly estimate the contribution of each parameter in the model retrieval, producing ill-posed problems. This particu-

larly applies to the parameters having a small effect on the whole spectrum, such as C_{x}. Consequently, to correctly estimate C_{x}, either a reference (unstressed) spectrum or the inclusion of *a-priori* information is needed; similar to the case of ΔPRI, as discussed above. In this study we use reference spectra, measured for each investigated sample.

In the retrieval procedure, we used a simple cost function (the squared spectral difference), and narrowed down the spectral region to the VIS in order to increase the weight of the parameters of interest (C_{x}). It was necessary in order to prevent parameters that affect a broad spectral range, such as N and C_{w}, to dominate the cost function. An alternative to the applied narrowing of the spectral range is to attribute weights to specific wavelengths in the cost function. The retrieval might be also improved by selecting a different retrieval algorithm, as reviewed in Rivera et al. (2013); Verrelst et al. (2014), or strategy (Ali et al., 2016; Jay et al., 2016; Li et al., 2018; Li and Wang, 2011).

Another important factor in the accuracy of parameter estimations is spectral quality of the measurements. Our model sensitivity analysis shows that the chosen instrument noise level (SNR of 500) did not significantly perturb the retrieval of C_{x}, especially because most instruments used provide an even better SNR in the VIS. The error propagation in the retrieved parameters for photosynthetic pigments was about 10%, which is comparable to other studies, and for C_{x} the bias appeared to be minimal, only $\pm 3\%$.

The left singular vector for C_{x} suggests that 3 highly specific wavelengths should be used for the retrieving of C_{x}. Since the inner product of this vector with a given spectrum is highly sensitive to C_{x} and not to the other parameters, it could be used as an algorithm to estimate C_{x}. However, for such an algorithm to work operationally, the actual noise level of the measurement instrument is very important.

Fluspect simulations are directional-hemispherical. On the other hand, Dataset 1, used for calibration of K_{car0} and K_{car1}, is bidirectional; it assumes that the leaf is bi-Lambertian while most real leaves are not. As discussed in Vilfan et al. (2016), a common outcome is an overestimation of leaf R, which may cause an

inaccurate estimation of model parameters that affect R, particularly in the NIR region. Because we describe the xanthophyll de-epoxidation as a relative change in the total carotenoid absorption spectrum, only the conservation of spectral shape must be ensured, as compared to the integrating sphere measurements. FluoWat leaf clip measurements show a systematic deviation of 2% lower R values compared to the integrating sphere measurements, which could be explained by the clip not measuring the specular reflection (Luis Alonso, personal communication). Moreover, research shows (Bousquet et al., 2005; Jay et al., 2016) that the effect of diffuse and directional component on bidirectional measurements is highly wavelength independent in the VIS: the shape of the spectra in the region between 500 and 600 nm is relatively conservative, with increasing wavelength dependence at wavelengths below 520 nm. This is further supported by our results, where the accuracy of C_{x} retrieval was highest for Dataset 3 (Fig. 4), measured with an integrated sphere, and the general accuracy was very good (RRMSE of $\pm 1\%$) above 520 nm. These results also indicate, that C_{x} can be retrieved with different measuring techniques. This is important, as leaf clips coupled to spectrometers are easier to operate, and they allow for measurements of solar induced chlorophyll fluorescence spectra, which provides means to study the two dynamic leaf spectral features simultaneously.

5.3. Implications for future applications: Fluspect-CX in SCOPE

Most of the published studies have focused on changes in R only. The dynamics of green T is more difficult to measure, because its detection depends greatly on leaf thickness and pigment content. Nonetheless, in the simulations and interpretation of whole canopy measurements, it is necessary to include T. The Fluspect-CX model fills this gap. Although the SACs were calibrated to R data only, the model also simulates T, which, however, needs further validation efforts.

The need for a reference spectrum or *a-priori* information, reduces the direct applicability of both ΔPRI and C_{x}. Nonetheless, relating C_{x} to NPQ via a simple linear equation provides means to further (1) couple Fluspect-CX to a

biochemical routine, such as an extended Farquhar's photosynthesis model (Van der Tol et al., 2014), and to (2) implement Fluspect-CX into the model SCOPE.

By including the dynamic green R into SCOPE, we were able to simulate the top-of-canopy PRI in a multi-angular sun-to-sensor geometry. A preliminary example indicates (forward simulation, Figure 8), that the model is able to separate the directional and physiological effects on the top-of-canopy PRI, which is a crucial requirement for up-scaling the PRI index from leaf to the canopy, and even further to landscape and global levels, using satellite observations. The R directional effects are quite pronounced in the top-of-canopy PRI values: even if the xanthophyll cycle effect is not included in the model, some 'PRI' angular change is still generated due to the directional effects alone. These findings are in accordance with literature Drolet et al. (2005); Hall et al. (2008); Hilker et al. (2008) and call for further investigation.

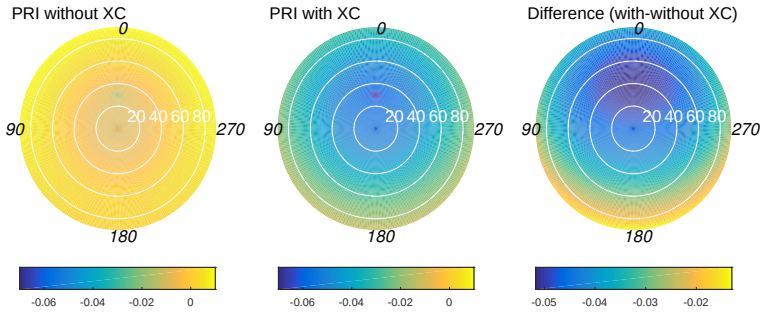

Figure 8: Hemispherical graphs of top-of-canopy PRI: without the xanthophyll cycle (XC) effect (left), with the xanthophyll cycle effect included in the model (middle) and the difference between the two (right) as a function of viewing zenith angle and viewing azimuth angle (relative to the solar azimuth). Zenith angle varies with the radius, the azimuth angle (in italic) increases while rotating anticlockwise from north. The sky was assumed clear and homogeneous, and the solar zenith angle was 30°.

6. Conclusions

This study demonstrates that dynamic changes in green R over short periods of time can be simulated and retrieved over a broad band from 515 to 565 nm

with a single new parameter, C_x.

With Fluspect-CX one could retrieve C_x for any R spectrum, as long as the two conditions are met: 1) the retrieval is done in at least two steps: over the whole measured spectrum, and further in the spectral range of carotenoid absorption; and 2) either a reference (unstressed) spectrum or certain prior information is provided.

By linking NPQ with C_x, we were able to create a connection between the radiative transfer model of the leaf (Fluspect-CX), and the canopy model SCOPE, such that the PRI can be simulated on both the leaf and canopy scale. The introduction of the photochemistry driven leaf reflectance dynamics into the models Fluspect and SCOPE thus presents new opportunities for the study of photosynthesis: 1) The PRI effect can be up-scaled to the canopy, and the directional and physiological effects on the canopy PRI can be separated; 2) Dynamic green R and chlorophyll fluorescence changes can be simulated simultaneously. When related to biochemical routines, this should enable us to better decouple the contributions of NPQ, PQ and fluorescence to the process of photosynthesis; 3) With the inclusion of C_{ant} and C_x, these features should allow for monitoring of leaf and canopy properties and development on both shorter and longer time scales, but also between species.

Acknowledgements

The research presented in this paper is funded by the Netherlands Organization for Scientific Research (NWO) in the frame of the Earth and Life Sciences (ALW) division, project ALW-GO/13-32. We thank Maria Pilar Cendrero-Mateo for the organisation and support with the collection of Dataset 1. We thank Luis Alonso for his advice and information provided on the FluoWat leaf clip measurements. Dataset 3 was collected with support from an Australian Research Council Discovery grant "AirLIFT" (DP140101488). We thank Barry Osmond for his assistance with collecting measurements and John Evans for the use of the Licor Integrating sphere. Technical support for the LIFT instrument

was provided by Zbigniew Kolber. For HPLC and other measurements we thank Johanna Turnbull and Melinda Waterman. This research was completed as part of Rhys Wyber's PhD and partially funded through an Australian Government Research Training Program Scholarship.

References

Adams, W.W., Demmig-Adams, B., 1992. Operation of the xanthophill cycle in higher plants in response to diurnal changes in incident sunlight. Planta 186, 390–398.

Ali, A.M., Darvishzadeh, R., Skidmore, A.K., van Duren, I., Heiden, U., Heurich, M., 2016. Estimating leaf functional traits by inversion of PROSPECT: Assessing leaf dry matter content and specific leaf area in mixed mountainous forest. International Journal of Applied Earth Observation and Geoinformation 45, 66–76. doi:10.1016/j.jag.2015.11.004.

Barton, C.V.M., North, P.R.J., 2001. Remote sensing of canopy light use efficiency using the photochemical reflectance index: Model and sensitivity analysis. Remote Sensing of Environment 78, 264–273.

Björkman, O., Demmig-Adams, B., 1995. Regulation of photosynthetic light energy capture, conversion, and dissipation in leaves of higher plants, in: Ecophysiology of photosynthesis. Springer, pp. 17–47.

Bousquet, L., Lachérade, S., Jacquemoud, S., Moya, I., 2005. Leaf BRDF measurements and model for specular and diffuse components differentiation. Remote Sensing of Environment 98, 201–211. doi:10.1016/j.rse.2005.07.005.

Brugnoli, E., Björkman, O., 1992. Chloroplast movements in leaves: Influence on chlorophyll fluorescence and measurements of light-induced absorbance changes related to ΔpH and zeaxanthin formation. Photosynthesis Research 32, 23–35. doi:10.1007/BF00028795.

Demmig-Adams, B., 1990. Carotenoids and photoprotection in plants: A role for the xanthophyll zeaxanthin. Biochimica et Biophysica Acta (BBA) - Bioenergetics 1020, 1–24. doi:http://dx.doi.org/10.1016/0005-2728(90)90088-L.

Demmig-Adams, B., Adams, W.W., 2006. Tansley review:Photoprotection in an ecological context: the remarkable complexity of thermal energy dissipation. New Phytologist 172, 11–21.

Drolet, G.G., Huemmrich, K.F., Hall, F.G., Middleton, E.M., Black, T.A., Barr, A.G., Margolis, H.A., 2005. A MODIS-derived photochemical reflectance index to detect inter-annual variations in the photosynthetic light-use efficiency of a boreal deciduous forest. Remote Sensing of Environment 98, 212–224.

Evain, S., Flexas, J., Moya, I., 2004. A new instrument for passive remote sensing: 2. Measurement of leaf and canopy reflectance changes at 531 nm and their relationship with photosynthesis and chlorophyll fluorescence. Remote Sensing of Environment 91, 175–185. doi:10.1016/j.rse.2004.03.012.

Féret, J.B., François, C., Asner, G.P., Gitelson, A.A., Martin, R.E., Bidel, L.P., Ustin, S.L., le Maire, G., Jacquemoud, S., 2008. PROSPECT-4 and 5: Advances in the leaf optical properties model separating photosynthetic pigments. Remote Sensing of Environment 112, 3030–3043. doi:10.1016/j.rse.2008.02.012.

Féret, J.B., Gitelson, A., Noble, S., Jacquemoud, S., 2017. PROSPECT-D: Towards modeling leaf optical properties through a complete lifecycle. Remote Sensing of Environment 193, 204–215. doi:10.1016/j.rse.2017.03.004.

Fréchette, E., Chang, C.Y.Y., Ensminger, I., 2016. Photoperiod and temperature constraints on the relationship between the photochemical reflectance index and the light use efficiency of photosynthesis in Pinus strobus. Tree Physiology 36, 311–324. doi:10.1093/treephys/tpv143.

Gamon, J.A., Field, C.B., Bilger, W., Björkman, O., Fredeen, A.L., Peñuelas, J., 1990. Remote sensing of the xanthophyll cycle and chlorophyll fluorescence in sunflower leaves and canopies. Oecologia 85, 1–7. doi:10.1007/BF00317336.

Gamon, J.A., Peñuelas, J., Field, C.B., 1992. A narrow-waveband spectral index that tracks diurnal changes in photosynthetic efficiency. Remote Sensing of Environment 41, 35–44. doi:10.1016/0034-4257(92)90059-S.

Gamon, J.A., Serrano, L., Surfus, J.S., 1997. The photochemical reflectance index: an optical indicator of photosynthetic radiation use efficiency across species, functional types, and nutrient levels. Oecologia 112, 492–501. doi:10.1007/s004420050337.

Garbulsky, M.F., Peñuelas, J., Gamon, J., Inoue, Y., Filella, I., 2011. The photochemical reflectance index (PRI) and the remote sensing of leaf, canopy and ecosystem radiation use efficiencies. A review and meta-analysis. Remote Sensing of Environment 115, 281–297. doi:10.1016/j.rse.2010.08.023.

García-Plazaola, J., Matsubara, S., Osmond, C.B., 2007. The lutein epoxide cycle in higher plants: Its relationships to other xanthophyll cycles and possible functions. Functional Plant Biology 34, 759–773. doi:10.1071/FP07095.

Gastellu-Etchegorry, J.P., Lauret, N., Yin, T., Landier, L., Kallel, A., Malenovský, Z., Al Bitar, A., Aval, J., Benhmida, S., Qi, J., Medjdoub, G., Guilleux, J., Chavanon, E., Cook, B., Morton, D., Chrysoulakis, N., Mitraka, Z., 2017. DART: Recent advances in remote sensing data modeling with atmosphere, polarization, and chlorophyll fluorescence. IEEE Journal of Selected Topics in Applied Earth Observations and Remote Sensing 10, 2640–2649. doi:10.1109/JSTARS.2017.2685528.

Gilmore, A., Yamamoto, H., 1993. Linear models relating xanthophylls and lumen acidity to non-photochemical fluorescence quenching. Evidence that antheraxanthin explains zeaxanthin-independent quenching. Photosynthesis Research 35, 67–78. doi:10.1007/BF02185412.

Gitelson, A.A., Gamon, J.A., Solovchenko, A., 2017. Multiple drivers of seasonal change in PRI: Implications for photosynthesis 1. Leaf level. Remote Sensing of Environment 191, 110–116. doi:10.1016/j.rse.2016.12.014.

Haboudane, D., Miller, J.R., Tremblay, N., Zarco-Tejada, P.J., Dextraze, L., 2002. Integrated narrow-band vegetation indices for prediction of crop chlorophyll content for application to precision agriculture. Remote Sensing of Environment 81, 416–426. doi:10.1016/S0034-4257(02)00018-4.

Hall, F.G., Hilker, T., Coops, N.C., Lyapustin, A., Huemmrich, K.F., Middleton, E., Margolis, H., Drolet, G., Black, T.A., 2008. Multi-angle remote sensing of forest light use efficiency by observing PRI variation with canopy shadow fraction. Remote Sensing of Environment 112, 3201–3211. doi:10.1016/j.rse.2008.03.015.

Harris, A., Gamon, J.A., Pastorello, G.Z., Wong, C.Y.S., 2014. Retrieval of the photochemical reflectance index for assessing xanthophyll cycle activity: a comparison of near-surface optical sensors. Biogeosciences 11, 6277–6292. doi:10.5194/bg-11-6277-2014.

Hilker, T., Coops, N.C., Hall, F.G., Black, T.A., Wulder, M.A., Nesic, Z., Krishnan, P., 2008. Separating physiologically and directionally induced changes in PRI using BRDF models. Remote Sensing of Environment 112, 2777–2788. doi:10.1016/j.rse.2008.01.011.

Hmimina, G., Dufrêne, E., Soudani, K., 2014. Relationship between photochemical reflectance index and leaf ecophysiological and biochemical parameters under two different water statuses: Towards a rapid and efficient correction method using real-time measurements. Plant, Cell and Environment 37, 473–487. doi:10.1111/pce.12171.

Horton, P., Ruban, A.V., Walters, R.G., 1994. Regulation of Light Harvesting in Green Plants (Indication by Nonphotochemical Quenching of Chlorophyll Fluorescence). Plant Physiology 106, 415.

Jacquemoud, S., Baret, F., 1990. PROSPECT: A model of leaf optical properties spectra. Remote Sensing of Environment 34, 75–91.

Jahns, P., Holzwarth, A.R., 2012. The role of the xanthophyll cycle and of lutein in photoprotection of photosystem II. Biochimica et Biophysica Acta (BBA) - Bioenergetics 1817, 182–193. doi:10.1016/j.bbabio.2011.04.012.

Jay, S., Bendoula, R., Hadoux, X., Féret, J.B., Gorretta, N., 2016. A physically-based model for retrieving foliar biochemistry and leaf orientation using close-range imaging spectroscopy. Remote Sensing of Environment 177, 220–236. doi:10.1016/j.rse.2016.02.029.

Königer, M., Bollinger, N., 2012. Chloroplast movement behavior varies widely among species and does not correlate with high light stress tolerance. Planta 236, 411–426. doi:10.1007/s00425-012-1619-9.

Kováč, D., Malenovský, Z., Urban, O., Špunda, V., Kalina, J., Ač, A., Kaplan, V., Hanuš, J., 2013. Response of green reflectance continuum removal index to the xanthophyll de-epoxidation cycle in Norway spruce needles. Journal of Experimental Botany 64, 1817–1827. doi:10.1093/jxb/ert069.

Kováč, D., Navrátil, M., Malenovský, Z., Štroch, M., Špunda, V., Urban, O., 2012. Reflectance continuum removal spectral index tracking the xanthophyll cycle photoprotective reactions in Norway spruce needles. Functional Plant Biology 39, 987–998. doi:10.1071/FP12107.

Li, D., Cheng, T., Jia, M., Zhou, K., Lu, N., Yao, X., Tian, Y., Zhu, Y., Cao, W., 2018. PROCWT: Coupling PROSPECT with continuous wavelet transform to improve the retrieval of foliar chemistry from leaf bidirectional reflectance spectra. Remote Sensing of Environment 206, 1–14. doi:10.1016/j.rse.2017.12.013.

Li, P., Wang, Q., 2011. Retrieval of leaf biochemical parameters using PROSPECT inversion: A new approach for alleviating ill-posed problems.

IEEE Transactions on Geoscience and Remote Sensing 49, 2499–2506. doi:10.1109/TGRS.2011.2109390.

Lichtenthaler, H.K., Buschmann, C., 2001. Chlorophylls and Carotenoids : Measurement and Characterization by UV-VIS. Current Protocols in Food Analytical Chemistry F4.3.1-F4., 1–8. doi:10.1002/0471142913.

Magney, T.S., Vierling, L.A., Eitel, J.U., Huggins, D.R., Garrity, S.R., 2016. Response of high frequency Photochemical Reflectance Index (PRI) measurements to environmental conditions in wheat. Remote Sensing of Environment 173, 84–97. doi:10.1016/j.rse.2015.11.013.

Malenovský, Z., Ufer, C., Lhotáková, Z., Clevers, J.G.P.W., Schaepman, M.E., Albrechtová, J., Cudlín, P., Z Malenovský Z Lhotáková, J G P W Clevers, M E Schaepman, J Albrechtová & P Cudlín, C.U., Z Malenovský Z Lhotáková, J G P W Clevers, M E Schaepman, J Albrechtová & P Cudlín, C.U., 2006. A new hyperspectral index for chlorophyll estimation of a forest canopy: Area under curve normalised to maximal band depth between 650-725 nm. EARSeL eProceedings, 5, 161–172. doi:10.5167/uzh-62112.

Matsubara, S., Naumann, M., Martin, R., Nichol, C., Rascher, U., Morosinotto, T., Bassi, R., Osmond, B., 2005. Slowly reversible de- epoxidation of lutein-epoxide in deep shade leaves of a tropical tree legume may 'lock-in' lutein-based photoprotection during acclimation to strong light, in: Journal of Experimental Botany, Oxford University Press. pp. 461–468. URL: https://academic.oup.com/jxb/article-lookup/doi/10.1093/jxb/eri012, doi:10.1093/jxb/eri012.

Miller, J.R., Berger, M., Goulas, Y., Jacquemoud, S., Louis, J., Mohammed, G., Moise, N., Moreno, J., Moya, I., Pedrós, R., 2005. Development of a vegetation fluorescence canopy model. ESTEC Contract .

Niyogi, K.K., Björkman, O., Grossman, A.R., 1997. The roles of specific xanthophylls in photoprotection. Proceedings of the National Academy of Sciences 94, 14162–14167.

Niyogi, K.K., Grossman, A.R., Björkman, O., 1998. Arabidopsis Mutants Define a Central Role for the Xanthophyll Cycle in the Regulation of Photosynthetic Energy Conversion. The Plant Cell Online 10, 1121–1134. doi:10.1105/tpc.10.7.1121.

Panigada, C., Rossini, M., Meroni, M., Cilia, C., Busetto, L., Amaducci, S., Boschetti, M., Cogliati, S., Picchi, V., Pinto, F., Marchesi, A., Colombo, R., 2014. Fluorescence, PRI and canopy temperature for water stress detection in cereal crops. International Journal of Applied Earth Observation and Geoinformation 30, 167–178. doi:http://dx.doi.org/10.1016/j.jag.2014.02.002.

Peñuelas, J., Llusia, J., Pinol, J., Filella, I., 1997. Photochemical reflectance index and leaf photosynthetic radiation-use-efficiency assessment in Mediterranean trees. International Journal of Remote Sensing 18, 2863–2868.

Pogson, B., McDonald, K.A., Truong, M., Britton, G., DellaPenna, D., 1996. Arabidopsis carotenoid mutants demonstrate that lutein is not essential for photosynthesis in higher plants. Plant Cell 8, 1627–1639. doi:10.1105/tpc.8.9.1627.

Porcar-Castell, A., Tyystjärvi, E., Atherton, J., Van der Tol, C., Flexas, J., Pfündel, E.E., Moreno, J., Frankenberg, C., Berry, J.A., 2014. Linking chlorophyll a fluorescence to photosynthesis for remote sensing applications: Mechanisms and challenges. Journal of Experimental Botany 65, 4065–4095. doi:10.1093/jxb/eru191.

Rivera, J.P., Verrelst, J., Leonenko, G., Moreno, J., 2013. Multiple cost functions and regularization options for improved retrieval of leaf chlorophyll content and LAI through inversion of the PROSAIL model. Remote Sensing 5, 3280–3304. doi:10.3390/rs5073280.

Ruban, A.V., 2016. Nonphotochemical Chlorophyll Fluorescence Quenching: Mechanism and Effectiveness in Protecting Plants from Photodamage. Plant physiology 170, 1903–16. doi:10.1104/pp.15.01935.

Sims, D.A., Gamon, J.A., 2002. Relationships between leaf pigment content and spectral reflectance across a wide range of species, leaf structures and developmental stages. Remote Sensing of Environment 81, 337–354. doi:10.1016/S0034-4257(02)00010-X, arXiv:arXiv:1011.1669v3.

Suetsugu, N., Higa, T., Wada, M., 2017. Ferns, mosses and liverworts as model systems for light-mediated chloroplast movements. Plant Cell and Environment 40, 2447–2456. doi:10.1111/pce.12867.

Ustin, S.L., Gitelson, a.a., Jacquemoud, S., Schaepman, M.E., Asner, G.P., Gamon, J.A., Zarco-Tejada, P.J., 2009. Retrieval of folair information about plant pigment systems from high resolution spectroscopy. Remote Sensing of Environment 113, S67–S77.

Van der Tol, C., Berry, J.A., Campbell, P.K., Rascher, U., 2014. Models of fluorescence and photosynthesis for interpreting measurements of solar-induced chlorophyll fluorescence. Journal of Geophysical Research G: Biogeosciences 119, 2312–2327. doi:10.1002/2014JG002713.

Van der Tol, C., Verhoef, W., Timmermans, J., Verhoef, A., Su, Z., 2009. An integrated model of soil-canopy spectral radiances, photosynthesis, fluorescence, temperature and energy balance. Biogeosciences 6, 3109–3129. doi:10.5194/bg-6-3109-2009.

Verrelst, J., Rivera, J.P., Leonenko, G., Alonso, L., Moreno, J., 2014. Optimizing LUT-based RTM inversion for semiautomatic mapping of crop biophysical parameters from sentinel-2 and -3 data: Role of cost functions. IEEE Transactions on Geoscience and Remote Sensing 52, 257–269. doi:10.1109/TGRS.2013.2238242.

Vilfan, N., Van der Tol, C., Muller, O., Rascher, U., Verhoef, W., 2016. Fluspect-B: A model for leaf fluorescence, reflectance and transmittance spectra. Remote Sensing of Environment 186, 596–615. doi:10.1016/j.rse.2016.09.017.

Wong, C.Y.S., Gamon, J.A., 2015. Three causes of variation in the photochemical reflectance index (PRI) in evergreen conifers. The New phytologist 206, 187–95. doi:10.1111/nph.13159.

Wyber, R., Malenovský, Z., Ashcroft, M.B., Osmond, B., Robinson, S.A., 2017. Do daily and seasonal trends in leaf solar induced fluorescence reflect changes in photosynthesis, growth or light exposure? Remote Sensing 9, 604. doi:10.3390/rs9060604.

Zhang, Q., M. Chen, J., Ju, W., Wang, H., Qiu, F., Yang, F., Fan, W., Huang, Q., ping Wang, Y., Feng, Y., Wang, X., Zhang, F., 2017. Improving the ability of the photochemical reflectance index to track canopy light use efficiency through differentiating sunlit and shaded leaves. Remote Sensing of Environment 194, 1–15. doi:10.1016/j.rse.2017.03.012.